WARSAW UNIVERSITY OF TECHNOLOGY Index 351733
FACULTY OF CIVIL ENGINEERING
COMMITTEE FOR CIVIL AND WATER ENGINEERING
POLISH ACADEMY OF SCIENCES ISSN 1230-2945

DOI: 10.24425/ace.2025.153321
ARCHIVES OF CIVIL ENGINEERING
Vol. LXXI ISSUE 1 2025

pp. 65 –81

Research paper

Study on deformation of layered rock tunnel based on material point method

Jingjie Pang[1], Zhenhua Xing[2], Yang Li[3], Binwei Xia[4], Gexin Wan[5], Shusen Wang[6], Kang Fu[7]

Abstract: The stability problems of layered rock mass are frequently encountered in tunnel and underground engineering. Affected by bedding plane, the mechanical properties of surrounding rock show obvious anisotropy, which makes its failure characteristics more complicated. Therefore, it is essential to clarify the deformation and damage characteristics of the tunnel in layered rock for the safe and efficient development. In this study, a numerical simulation tool based on material point method and strain softening model is used to establish the plane strain model of tunnel in layered rock, and the deformation process of the tunnel with different dip angles and different rock thickness is studied. The results show that: 1) Compared with the physical simulation test, it is proved that the tool used can simulate the complex process of tunnel deformation and instability, and effectively realize delamination, shear slip and rock fracture in the failure process of tunnel in layered rock; 2) The bedding plane has a significant influence on the failure characteristics of surrounding rock, and the damaged area increases significantly on the bedding plane, cracks are always concentrated in the direction perpendicular to the bedding plane, and the smaller the thickness of the rock layer, the larger the damage area of the surrounding rock; 3) With the increase of joint angle, the number of failure points presents a U-shaped trend, and the decrease of rock thickness will lead to an increase in the number of failure points and a decrease in the percentage of shear failure points.

Keywords: fracture field, layered rock mass, material point method, stability of surrounding rock

[1]M.Eng., State Key Laboratory of Coal Mine Disaster Dynamics and Control, Chongqing University, Chongqing, China, e-mail: 1604024682@qq.com, ORCID: 0009-0001-2884-3777
[2]Eng., China Construction Third Engineering Bureau Group Co., Ltd, China Construction Third Engineering Bureau Group Co., Ltd, Wuhan, Hubei Province, China, e-mail: xingzhenhua202401@163.com, ORCID: 0009-0002-3137-6353
[3]Eng., Chongqing Expressway Wuyunkai Construction Co., Ltd, Chongqing Expressway Group Co., Ltd, Chongqing, China, e-mail: liyang202401@163.com, ORCID: 0009-0001-6313-9312
[4]Prof., PhD., Eng., State Key Laboratory of Coal Mine Disaster Dynamics and Control, Chongqing University, Chongqing, China, e-mail: xbwei33@cqu.edu.cn, ORCID: 0000-0002-8928-0461
[5]Eng., Chongqing Expressway Wuyunkai Construction Co., Ltd, Chongqing Expressway Group Co., Ltd, Chongqing, China, e-mail: wangexin202401@163.com, ORCID: 0009-0006-9643-2941
[6]Eng., China State Construction Railway Investment & Engineering Group Co., Ltd, China Construction Third Engineering Bureau Group Co., Ltd, Beijing, China, e-mail: wangshusen202401@163.com, ORCID: 0009-0002-3925-3016
[7]Eng., China State Construction Railway Investment & Engineering Group Co., Ltd, China Construction Third Engineering Bureau Group Co., Ltd, Beijing, China, e-mail: fukang202401@163.com, ORCID: 0009-0000-9002-3190

1. Introduction

Layered rock masses, as a complex geological formations frequently encountered in geotechnical and underground engineering, are widely distributed in the southwest, central, and other regions, which account for 77.3% of China's land and approximately 2/3 of the Earth's land surface [1]. Engineering practices have observed significant rock slip and bending damage in the surrounding rock of tunnels due to the presence of bedding plane [2]. This has led to a series of destabilizing accidents, such as the bottom drum of the back arch, rock spalling and lining cracking [3, 4], significantly reducing the stability of the tunnel. Therefore, accurately and intuitively predicting the damage process and deformation characteristics of the surrounding rock in tunnels is the main challenge in the construction or maintenance of the tunnels in layered rocks.

The anisotropic damage characteristics of layered rock masses are considered a significant risk factor in underground construction. Long-term geological tectonic action has substantially reduced the integrity of the rock body through the presence of joints, resulting in anisotropic deformation and strength characteristics [5, 6]. Research indicates that parameters such as rock layer thickness and joint angle influence macro fracture characteristics, detailed damage patterns, and the damage process of the surrounding rock [7, 8]. Furthermore, the excavation of underground chambers and tunnels represents a dynamic response process impacted by various factors, including topography, structure, and rock properties, leading to a particularly complex deformation and damage mechanism of the tunnel in layered rocks [9].

Over the years, scholars have utilized on-site tests [10], model experiments [11, 12], and numerical simulations [13–15] to investigate the damage characteristics of tunnels in layered rock and mitigate the risk of anisotropy in layered rock. Numerical simulation has emerged as an effective means for global scholars to assess the stability of tunnel, addressing the limitations of field testing and modeling experiments, including high cost, long cycle time, high risk, and reproducibility challenges. Li et al. [16] employed the finite element method (FEM) to analyze the plasticity characteristics and deformation law of the tunnels in layered rocks, yet they were unable to capture the crack extension process and crack initiation characteristics. Similarly, Do et al. [17] studied the impact of joint angle and lateral earth pressure coefficient on tunnel convergence using FEM, without visualizing the deformation and damage characteristics of the tunnel. Yin et al. [18] utilized the discrete element method (DEM) to model the simulation of layered rocks and found that the bond removal method (BRM) is better suited to depict the real macroscopic fracture surface, while the smooth joint method (SJM) can statistically characterize the number and distribution of cracks. However, neither method enabled the simultaneous acquisition of macroscopic crack evolution and fine-scale damage processes. Furthermore, numerical methods such as rock failure process analysis (RFPA) [19] and finite-discrete element method (FDEM) [20] have been employed to simulate the deformation and damage process of the tunnels or underground chambers in layered rocks. Yet, none effectively and intuitively simulated and calculated the shear-slip and bending damage processes of layered rock.

The above numerical simulation studies mainly use numerical methods based on the assumption of continuous deformation or discontinuous deformation, such as finite difference

method (FDM), FEM, and DEM. In the layered rock tunneling engineering, the damage of tunnels will occur in a variety of damage forms, such as rock slip, bending damage, composite damage and so on. Mechanical processes such as large deformation, large displacement, continuous change of unit boundaries within the material and contact are all involved [21]. The FDM is based on the Eulerian description and adopts equally divided fixed grids in the rectangular coordinate system, which does not have the problem of mesh deformation, but is more difficult to solve for complex geometries and boundaries; The computational region of the traditional FEM can be obtained by combining simple geometrical shapes according to different coupling methods, which can deal with complex boundaries and adapt to a variety of shapes, but it is difficult to be applied to the case of extremely large element deformation; The DEM can easily realize the conversion from continuum to discontinuity and has inherent advantages for nonlinear mechanical problems such as large deformation and damage, but it is limited by the shortcomings of insufficient computational accuracy and theoretical rigor, and cannot truly reflect the mechanism of the rock.

The Material Point Method (MPM) [22] is a meshless numerical computational technique founded on a hybrid Lagrange and Euler description. This method involves discretizing the continuum into a set of mass points with mass, representing the motion and deformation of an object, while the background grid does not carry any material information. It is only used for calculating the spatial derivative and solving the momentum equation, and the deformed grid will be abandoned, while the undeformed background grid will be used in the new time step, which makes it suited for addressing challenges associated with large deformation and crushing. To elucidate the deformation and damage characteristics of the tunnel in layered rocks, the entire process of delamination, shear-slip, and rock breakage of surrounding rock is simulated through a physical experimental model and the integration of the material point method and the strain-softening intrinsic model. The numerical simulation results exhibit high agreement with the physical experimental findings. Consequently, numerical simulations were conducted to investigate the deformation and damage characteristics of the tunnel in layered rocks, considering varying thicknesses of rock layers and different dips of joint faces. This enabled the clarification of the effects of layer thickness and joint angle on the displacement field, fissure field, and damage pattern of the tunnel. The study's outcomes provide a robust theoretical foundation for the construction and design of tunnels in layered rock.

2. MPM

2.1. Governing equation

The deformation of tunnels in layered rock is a complex mechanical process involving elastic-plastic deformation, rock damage, and rock slip. To describe the dynamics and deformation of elastic objects, the theory of elasticity is employed, primarily comprising the equations of motion Eq. (2.1), geometric equations Eq. (2.2), and the elastic constitutive equation Eq. (2.3).

$$\nabla\sigma + \rho\left(\boldsymbol{b} - \frac{\partial \boldsymbol{v}}{\partial t}\right) = 0 \tag{2.1}$$

$$\Delta\varepsilon = \frac{1}{2}\left[\nabla(\Delta\boldsymbol{u}) + \nabla^T(\Delta\boldsymbol{u})\right] \tag{2.2}$$

$$\Delta\sigma = \left(K - \frac{2}{3}G\right)\Delta\varepsilon_v + 2G\Delta\varepsilon_{dev} \tag{2.3}$$

where: σ – stress tensor (MPa), ε – strain tensor, ε_v – volumetric strain tensor, ε_{dev} – deviatoric strain tensor, ρ – density (kg/m^3), $\boldsymbol{b}$ – body force acting on the object (N/m^3), $\boldsymbol{v}$ – velocity (m/s), $\boldsymbol{u}$ – displacement (m), K – bulk modulus (MPa), G – shear modulus (MPa).

The failure modes of layered rock mass mainly include tensile failure and shear failure of bedrock, tensile failure and shear failure of bedding plane and their compound failure, etc. As shown in Fig. 1, the specified compressive stress is negative, line AB is Mohr–Coulomb shear yield criterion ($f^s = 0$), and line BC is tensile yield criterion ($\sigma_1 = \sigma_3$), when the material meets the conditions of tensile failure and shear failure at the same time, it can be regarded as a compound failure. Generally speaking, the tensile strength of rock materials is less than the shear strength ($c/\tan\phi$), so it is appropriate to use Mohr–Coulomb yield criterion with tensile cutoff to describe the failure of layered rock mass.

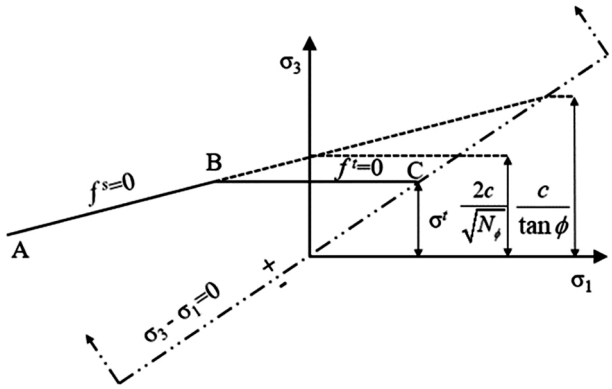

Fig. 1. Mohr–Coulomb criterion with tensile cutoff

$$f_s = \sigma_1 - N_\varphi\sigma_3 + 2c\sqrt{N_\varphi} \tag{2.4}$$

$$f_t = \sigma_3 - \sigma_t \tag{2.5}$$

where: f_s – shear yield strength (MPa), f_t – tensile yield strength (MPa), σ_1 – maximum principal stress (MPa), σ_3 – minimum principal stress (MPa), c – cohesive force (MPa), $N_\varphi = (1 + \sin\varphi)/(1 - \sin\varphi)$, φ – angle of internal friction (°), σ_t – tensile strength (MPa).

Plastic deformation arises when the local stress conditions meet the damage criterion. It embodies principal direction and amplitude, which are determined using the orthogonal flow law Eq. (2.6).

$$\Delta\varepsilon^p = \lambda\frac{\partial g}{\partial\sigma} \tag{2.6}$$

where: ε^p – plastic strain, λ – plastic multiplier, g – potential function, $g^s = \sigma_1 - \sigma_3 N_\psi$, $g^t = \sigma_3$, $N_\psi = \dfrac{1 + \sin\psi}{1 - \sin\psi}$, ψ – dilation angle (°), when we use the orthogonal flow law, $\psi = \varphi$.

In the simulation of multi-jointed rock damage and fracture process, a strain softening model was employed, and plastic deformation calculated by the model is large, so the separation of objects can be simulated in the area with large deformation of material points, resulting in macroscopic gaps, that is, physical fractures. It is worth emphasizing that no material points are deleted in this process.

$$\begin{cases} \phi = \phi_c, & \varepsilon_s^p > \varepsilon_{s,\max}^p \\ c = 0, & \varepsilon_s^p > \varepsilon_{s,\max}^p \\ \phi = \dfrac{\phi_0 - \phi_c}{\varepsilon_{s0}^p - \varepsilon_{s,\max}^p}\left(\varepsilon_s^p - \varepsilon_{s,\max}^p\right) + \phi_c, & \varepsilon_s^p > \varepsilon_{s,\max}^p \\ c = \dfrac{c_0}{\varepsilon_{s0}^p - \varepsilon_{s,\max}^p}\left(\varepsilon_s^p - \varepsilon_{s,\max}^p\right), & \varepsilon_s^p > \varepsilon_{s,\max}^p \end{cases} \tag{2.7}$$

$$\begin{cases} \sigma_t = 0, & \varepsilon_t^p > \varepsilon_{t,\max}^p \\ \sigma_t = \dfrac{\sigma_{t0}}{\varepsilon_{t0}^p - \varepsilon_{t,\max}^p}\left(\varepsilon_t^p - \varepsilon_{t,\max}^p\right), & \varepsilon_t^p < \varepsilon_{t,\max}^p \end{cases} \tag{2.8}$$

where: ε_{s0}^p, ε_{t0}^p – the initial shear and tensile plastic strain (–), $\varepsilon_{s,\max}^p$, $\varepsilon_{t,\max}^p$ – the critical shear and tensile plastic strain (–), ϕ_0, c_0, σ_{t0} – initial cohesion (MPa), initial friction angle (°) and initial tensile strength (Pa), ε_s^p, ε_t^p, ϕ, c and σ_t – shear plastic strain, tensile plastic strain, cohesion (MPa), friction angle (°) and tensile strength (MPa) under the current calculation step, ϕ_c – residual friction angle (°).

Therefore, the rock damage evolution process is described using a strain softening model Eq. (2.7) Eq. (2.8), employing plastic shear strain and tensile strain as softening factors to diminish rock strength. The softening process concludes upon reaching a critical plastic strain value. By facilitating the calculation of substantial plastic deformations, the strain softening model enables MPM to simulate object separation in regions of significant deformations, thereby generating visible cracks.

2.2. Solution process of MPM

MPM is a numerical computational technique that integrates Lagrange particles and Eulerian background grids. It is grounded on the principles of conservation of mass and momentum in continuum mechanics. This method discretizes the continuum into particles Eq. (2.9), with the particles containing all the matter-related information including density, velocity, and other pertinent data, while the background grid remains devoid of any information.

$$\rho(x_i) = \sum_{p=1}^{n_p} m_p \delta\left(x_i - x_{ip}\right) \tag{2.9}$$

where: n_p – total number of particles, m_p – mass (kg) of the particle p, δ – Dirac function, which has a value of zero at points other than zero and whose integral over the entire domain of definition is equal to 1, x_{ip} – coordinates of the position of the prime p.

The mutual mapping of information between the particles and the grid in MPM can be achieved using finite element shape functions to solve the equations of motion or to update the material information. In conventional MPM, a linear form function with a single particle of integration is typically employed. However, the center coordinates of a single particle do not entirely reflect its range, and the linear form function is discontinuous at the boundaries of the particle's influence range, potentially causing cross-cell errors and virtual cracks. To mitigate these issues, the authors cited the convective particle domain interpolation method by Ref. [23].

As illustrated in Fig. 2, the interpolation method represents the particle's geometry using a parallelogram shape. This parallelogram is defined by the concentric coordinate (x_p) and two structural vectors (R_1, R_2). The positions of the four corner points of the parallelogram particle can be determined using the concentric coordinate and the structural vector.

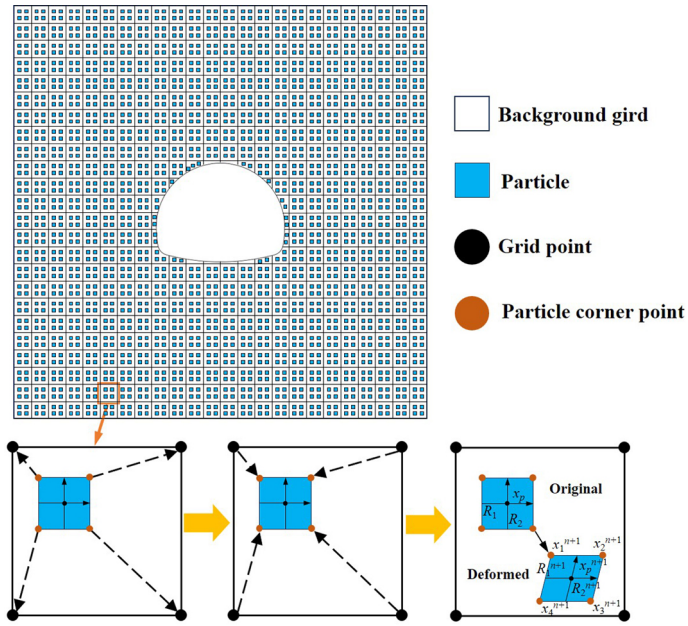

Fig. 2. Calculation process of MPM

The four corner points of a particle fully describe its influence range, enabling the construction of a continuous form function. This involves averaging the form function and their gradients at the particle center by using the four corners of each particle's domain. Then the velocity Eq. (2.10) and acceleration Eq. (2.11) of the grid nodes are updated:

$$v_I^{n+1} = \frac{M_I^n + \Delta t \cdot f_I^{n+1}}{m_I^n} \tag{2.10}$$

$$a_I^{n+1} = \frac{f_I^{n+1}}{m_I^n} \tag{2.11}$$

where: a – acceleration (m/s^2).

The particle displacement Eq. (2.12), velocity Eq. (2.13), and strain increment Eq. (2.14) are determined through interpolation, establishing a connection between the particle and node information.

$$u_p^{n+1} = u_p^{n+1} + \Delta t \sum_{I\varepsilon p} N_{Ic}^n v_I^{t+1} \tag{2.12}$$

$$v_p^{n+1} = v_p^n + \Delta t \sum_{I\varepsilon p} N_{Ic}^n a_I^{t+1} \tag{2.13}$$

$$\Delta\varepsilon_{p,ij}^{n+1} = \Delta t \sum_{I\varepsilon p} \frac{1}{2}\left(\frac{\partial N_{Ic}^n}{\partial j} v_{I,i}^{n+1} + \frac{\partial N_{Ic}^n}{\partial i} v_{I,i}^{n+1}\right) \tag{2.14}$$

where: N_{Ic}^n – the standard linear form function at the corner point of the particle.

Consequently, the update of the particle stress is structured in three steps: 1) employing the elastic constitutive equation Eq. (2.3) to compute the elastic stress; 2) detecting whether rock material points enter the plastic stage Eq. (2.4) Eq. (2.5); 3) after entering the plastic stage, adjusting the stress in accordance with the orthogonal flow law Eq. (2.6); 4) The accumulation of plastic strain will soften rock material points Eq. (2.7) Eq. (2.8), and further material points will be separated due to the decrease of strength, resulting in intuitive void areas.

3. Numerical solution

3.1. Numerical model

To assess the reliability of the material point method in simulating the deformation and instability process of layered rock tunnels, an 800 mm × 800 mm tunnel model, matching a similar model in the Ref. [24], is depicted in Fig. 3a. Here, the bedding plane is regarded as an extremely thin rock material with the same mechanical parameters as the bedrock, and its thickness is consistent with the cell grid size, the detailed mechanical parameters presented in Table 1. However, the bedding plane is easier to separate than bedrock in the plastic strain accumulation stage. The generated tunnel model is shown in Fig. 3b, where the bottom edge of the model is fixed and the remaining three edges are loaded with stress using a loading plate in the range of 0.1 MPa to 0.6 MPa, which is consistent with the method adopted in the Ref. [24].

Table 1. Calculated mechanical parameters of the model

Model Structure	**Density γ (kg/m^3)**	**Elastic Modulus E (Pa)**	**Poisson's Ratio μ**	**Cohesion c (Pa)**	**Angle of Internal Friction φ**	**Tensile Strength T (Pa)**	**Critical Plastic Strain**
Rock	2.1E+3	3.43E+8	0.26	4.5E+4	36°	2E+4	0.08
Joint plane	–	–	–	4.5E+4	36°	2E+4	0.04

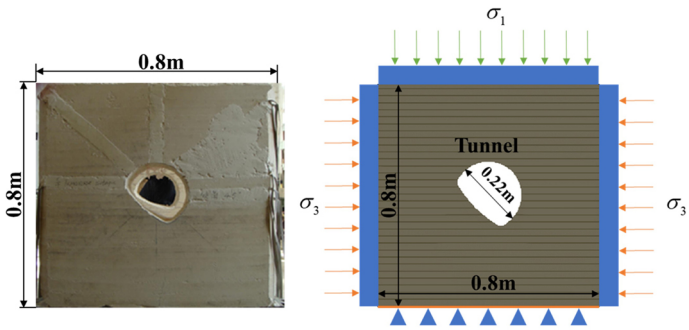

Fig. 3. Physical similarity model (a) and numerical model (b)

3.2. Verification

The numerical simulation results at 0.3 MPa were compared with the experimental results. In Fig. 4, the distribution of the plastic zone and the layout of the gauge lines are presented. Gauge line I is oriented perpendicular to the direction of the rock stratum, while Gauge line II is perpendicular to the roof arch of tunnel, with each gauge line being 1.6 times the radius of the tunnel in length. The radial and circumferential stresses at each point on the gauge lines were analysed. The plots of stress versus distance, depicted in Fig. 5 and Fig. 6, use the horizontal coordinate as the ratio of the distance from the gauge point to the wall to the tunnel diameter. The maximum circumferential stress distance from the tunnel wall closely matches the model experimental results, indicating that the damage range of the surrounding rock

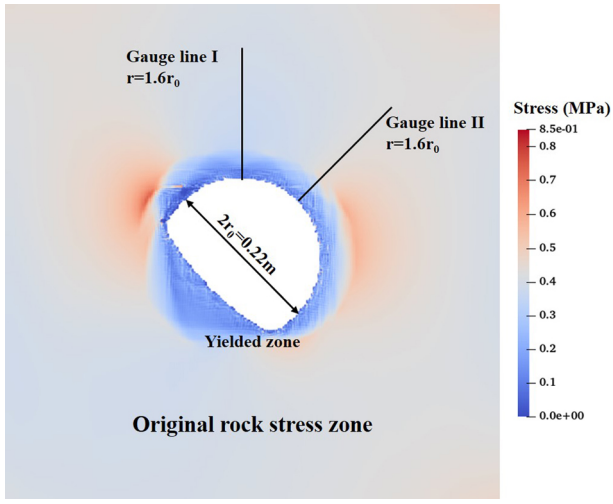

Fig. 4. Schematic diagram of the plastic zones and the layout of the gauge lines

under this stress loading condition aligns. Following stress reaching its peak, both numerical simulation and experimental results converge to the original rock stress zone. The average value of the ratio of the stress difference between the numerical simulation results and the experimental results is calculated to be 2.76%, which is acceptable.

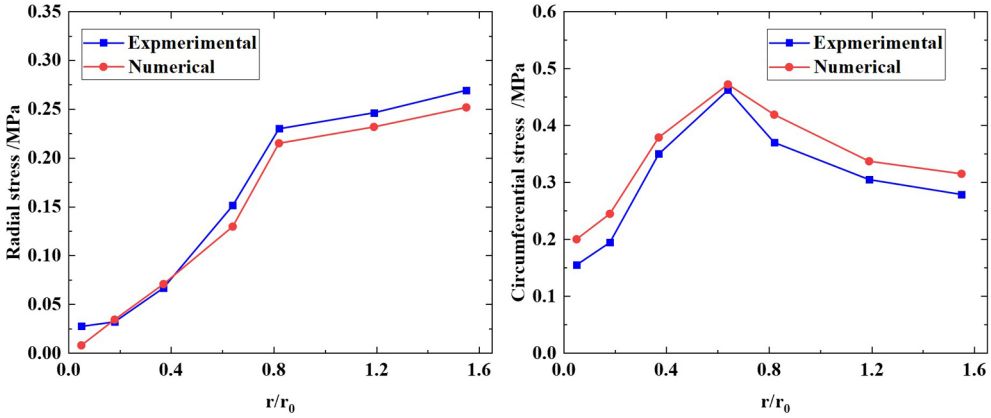

Fig. 5. Comparison between numerical results and experimental data of 45° model under gauge line ?: (a) Radial stress, (b) Circumferential

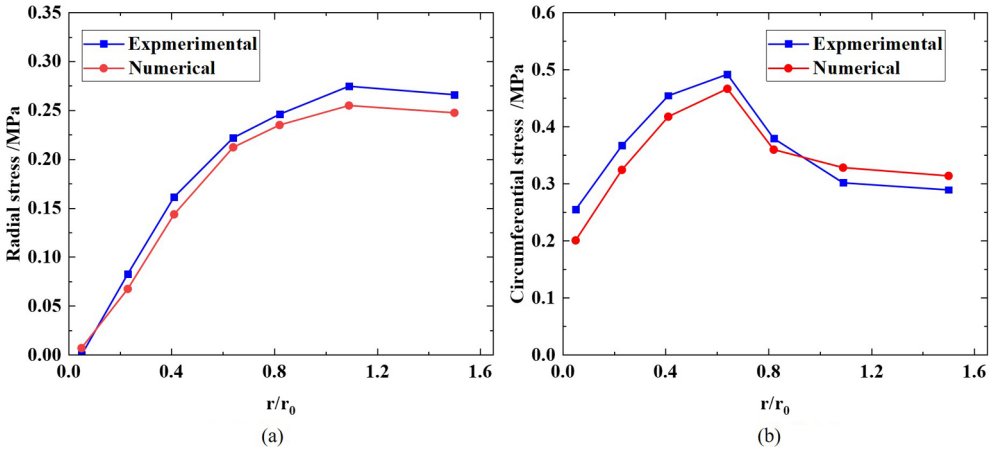

Fig. 6. Comparison between numerical results and experimental data of 45° model under gauge line ?: (a) Radial stress, (b) Circumferential

The model experiments utilized a pinhole camera placed inside the hole for real-time photographic monitoring, with the monitoring image captured at a distance far from the 45° model. Figure 7 presents the monitoring images under different stress conditions, intercepted and compared with the simulated images. At 0.3 MPa stress, no significant rock separation was observed in the experimental model, but partial separation of the left arch shoulder of the tunnel was observed in the numerical simulation. Under a 0.4 MPa stress state, more obvious

rock layer separation was visible in the right arch shoulder in the experimental setup, consistent with the numerical simulation results. Loading to a 0.5 MPa stress state, visible rock separation was apparent in the numerical simulation on the left arch shoulder of the model, without large through cracks, aligning with the experimental results. Upon reaching a 0.6 MPa stress state, notable separation and "X"-crack formation at the right arch shoulder were observed in the experimental model. The numerical simulation displayed inverted triangular blocks at the left arch shoulder but no falling, and "X" cracks perpendicular to the rock layer, consistent with the model experiments. These findings affirm the reliability of the numerical model established for the tunnel in layered rock in this study.

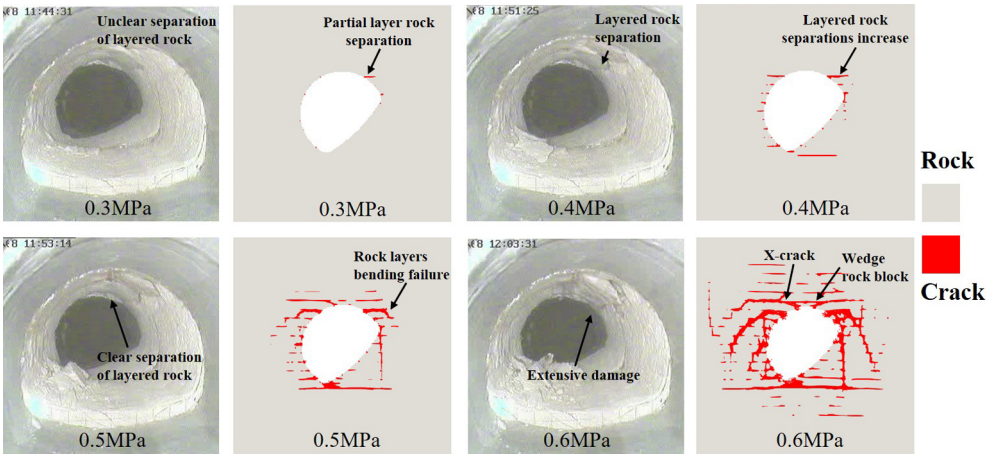

Fig. 7. Damage characteristics of the tunnel under different stress conditions

To elucidate the impact of rock thickness and joint angle on the deformation and damage characteristics of tunnels, the verified tunnel model served as the foundation for subjecting the tunnel to isometric loading. Stress loading, ranging from 0 to 0.6 MPa, was performed to simulate the failure process of the surrounding rock under varying joint angles and rock thicknesses. The detailed experimental scheme is presented in Table 2, while the boundary conditions and loading mode of the model are shown in Fig. 8.

Table 2. Table of numerical simulation program

Serial number	Joint angle α (°)	Rock thickness b (mm)	Stress condition σ (MPa)
1~5	0, 22.5, 45, 67.5, 90	20	0~0.6
6~9	0	10, 15, 20, 25	0~0.6
10	0	Intact rock	0~0.6

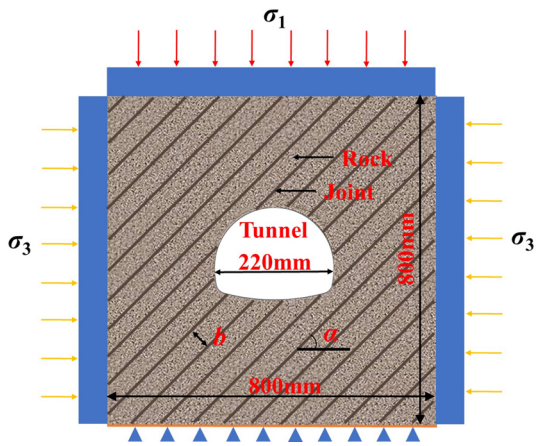

Fig. 8. Geometric model of tunnel loading damage

4. Discussion

4.1. Characterization of deformation

Figures 9 an 10 display the displacements for varying joint angles and rock thicknesses under a 0.6 MPa stress condition. Fig. 9 illustrates a shifted maximum displacement and altered distribution of the surrounding rock in the layered rock mass compared to the intact rock mass. For a rock layer angle of 0°, deformation primarily occurs at the right arch shoulder and left arch shoulder. At 22.5°, deformation is concentrated at the left arch shoulder and right arch foot; at 45°, deformation is uniformly distributed with distinct deformation in addition to the inverted arch; at 67.5°, deformation is mainly focused at the right arch side, right arch foot, and left arch side; and at 90°, symmetrically distributed tunnel deformation primarily occurs at the right arch side and left arch side. The deformation of surrounding rock is influenced by the rock layer angle, yet the deformation characteristics remain largely consistent. The tunnel deformation exhibits a phenomenon of inward convergence, and its direction is perpendicular to the angle of the bedding plane, aligning with the experimental results.

The thickness of the rock layer influences the maximum displacement of the tunnel surrounding rock, as depicted in Fig. 10. A reduction in the rock layer thickness results in the tunnel passing through more layers, leading to a continuous increase in the maximum displacement. Significant deformation occurs within the bedding plane between the arch and the arch shoulder due to the rock layer's orientation intersecting at a large angle with the inner tunnel wall, thus contributing to bending and deformation phenomena such as arch sinking and bottom bulge.

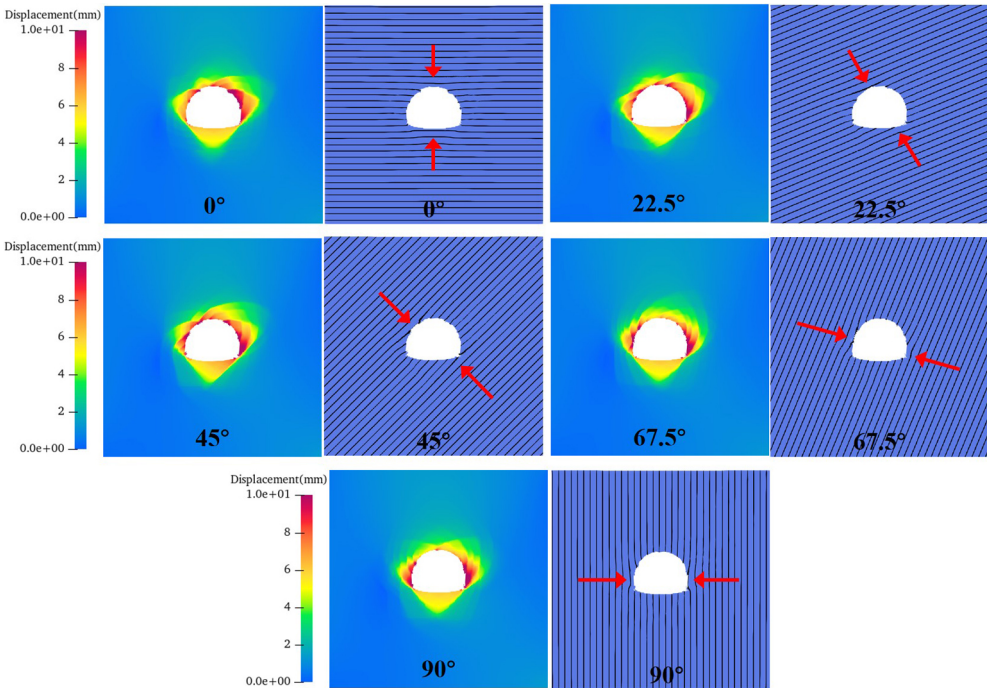

Fig. 9. Displacement and deformation characteristics of tunnel for different joint angles

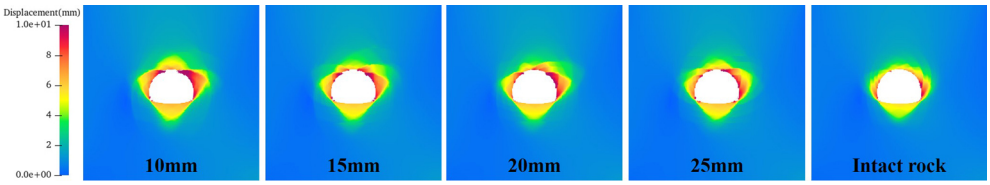

Fig. 10. Displacement of tunnel for different rock thicknesses

4.2. Crack extension

The results of extracting the crack map and shear plastic strain map at each stress level of the model with a layer thickness of 20mm and an angle of 45° are depicted in Fig. 11 and Fig. 12. Damage to the surrounding rock can be classified into three stages based on crack development. The first stage entails the initial deformation stage, in which the tunnel surrounding rock converges inward without any obvious cracks. The strain diagram reveals the presence of shear plastic strain around the tunnel, but it has not reached the maximum plastic strain, hence no cracks have formed. The second stage is characterized by the damage stage, during which the increase in surrounding rock stress leads to the emergence of off-layer phenomena in the rock layer, accompanied by the gradual generation of evident local cracks primarily along the extension of the joint surface; however, the length of the cracks does not

exceed the tunnel radius. The third stage represents the crack expansion stage, characterized by the rapid enlargement of the peripheral rock damage range, wherein the crack length significantly exceeds the tunnel radius, indicating obvious rock layer breakage and large-scale spalling in the surrounding rock.

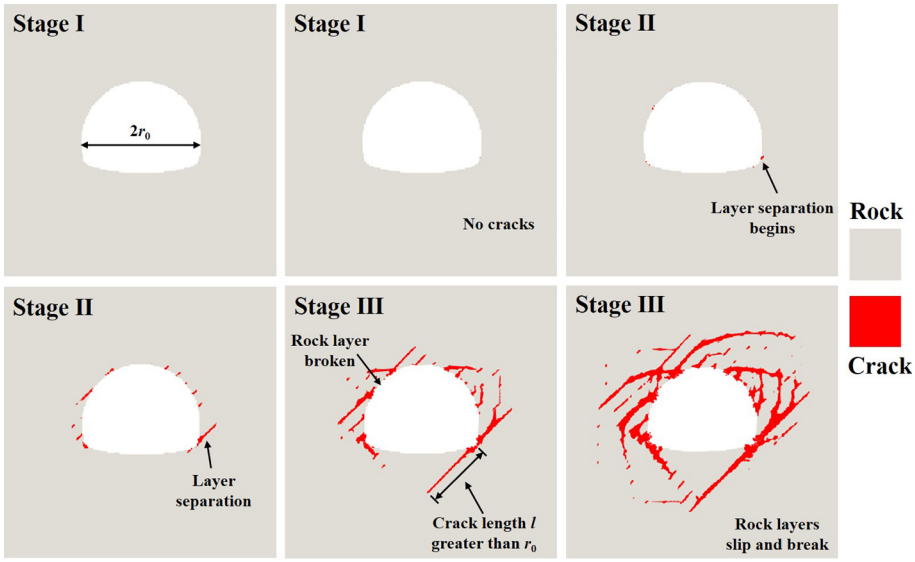

Fig. 11. Evolution of cracks in the surrounding rock

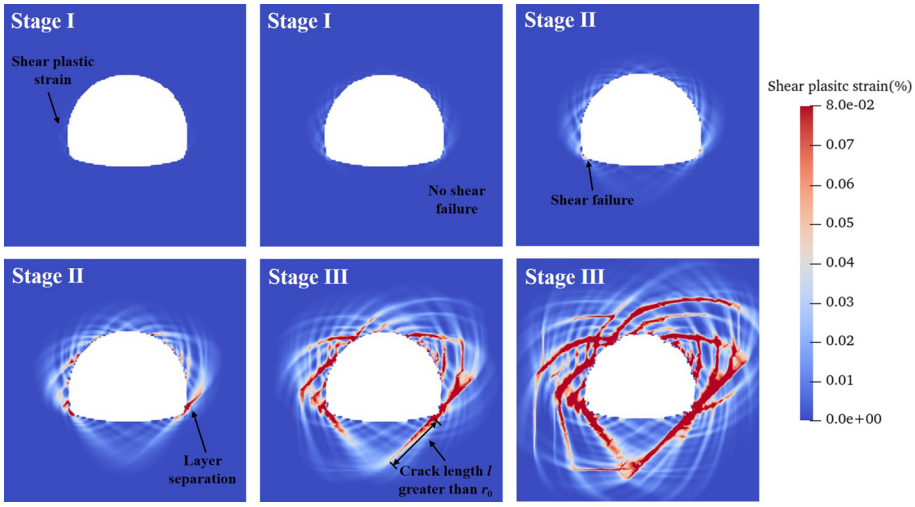

Fig. 12. Shear plastic strain diagram of surrounding rock

4.3. Analysis of damage patterns

In MPM software, when points exceed the material's maximum plastic strain, it is considered a failure. Exceeding the maximum value of shear plastic strain without surpassing the maximum value of tensile plastic strain indicates shear failure, while surpassing the maximum value of tensile plastic strain without exceeding the maximum value of shear plastic strain is classified as tensile failure. If both types of plastic strain reach their maximum values simultaneously, it is termed compound failure. The damage severity (D) is defined as the percentage ratio of the total number of failure points to the overall material points.

$$D = \frac{N_f}{N} \tag{4.1}$$

where: N_f – the total number of material points where failure occurred, N – the total number of material points.

Upon extraction of the plastic strain values from all material points and subsequent normalization, the damage severity and the number of failure points under various conditions are obtained, as depicted in Fig. 13 and Fig. 14, respectively. In Fig. 13, the damage severity for the tunnel surrounding rock demonstrates exponential escalation with increasing stress. During the initial deformation stage, the surrounding rock exhibits nearly zero damage, despite being plastically strained. Subsequent to the appearance of local cracks during the damage stage, the surrounding rock's damage increases steadily. However, the damage severity significantly accelerates during the crack extension stage, leading to increased crack depth and extensive destruction. Notably, at a consistent joint angle, the damage severity decreases markedly with the increased thickness, showing minimal susceptibility to joint angle.

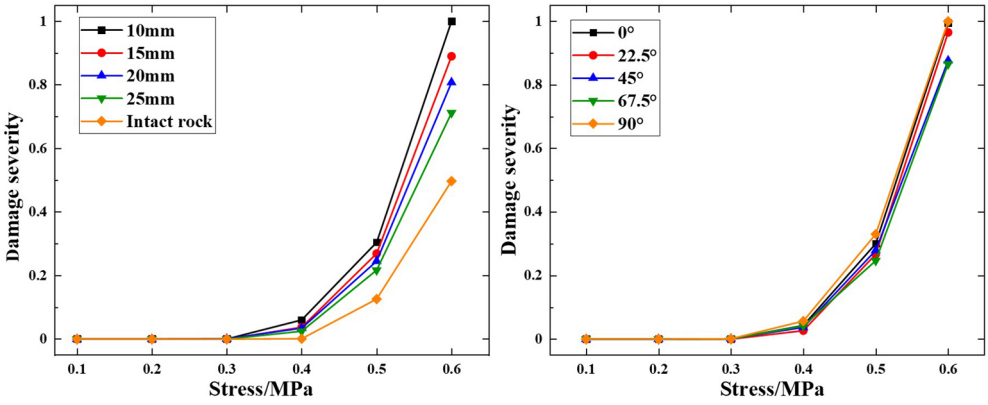

(a) (b)

Fig. 13. Influence of rock parameters (a) on the damage severity to the tunnel (b)

Analysis of Fig. 14 indicates that the predominant failure mode in the surrounding rock of the tunnel is shear failure. With increasing rock layer thickness, there is a corresponding increase in the proportion of shear failures. For instance, at 0.6MPa, the damage severity of

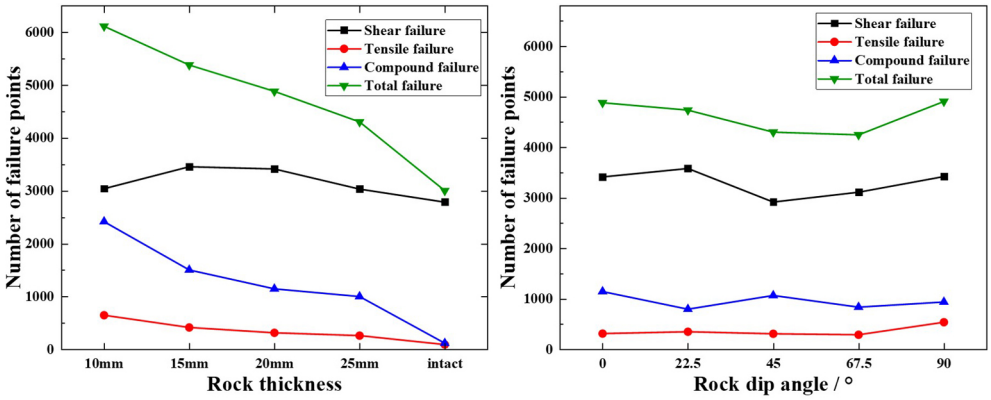

Fig. 14. Influence of rock parameters (a) on the amount of failure in the tunnel model (b)

intact rock mass is 1.1%, while the percentage of shear failure reaches about 92.7%. Moreover, the presence of joint surfaces contributes to an elevated occurrence of tensile and composite failures, significantly impacting the stability of the tunnel surrounding rock. As depicted in Fig. 14b, the distribution of failures takes the form of a "U" shape as the joint angle increases, with the lowest number of failures recorded at a joint angle of 67.5°. Conversely, a higher incidence of shear and tensile failures is observed when the rock layer angle is 90°. This phenomenon is attributed to the alignment of the rock layer angle with the direction of stress loading, leading to increased overall deformation and damage in the surrounding rock. Consequently, delamination and shear slippage become more prevalent, resulting in a higher occurrence of shear and tensile failures.

5. Conclusions

The research presented in this paper involves the establishment of a two-dimensional plane strain model of a tunnel in the layered rocks using a numerical simulation tool that relies on the material point method and the strain softening constitutive model. Subsequently, the numerical results are compared with existing experimental data to validate the method's efficacy in simulating the deformation of tunnel. Furthermore, a simulation study is conducted to investigate the damage process of the tunnel with varying thicknesses and joint angles, leading to the derivation of the following conclusions:

1. Through comparison with similar model experiments, it has been demonstrated that the numerical tool used is capable of simulating the complex process of tunnel deformation. This serves as evidence of the numerical tool's effectiveness in simulating dislocations, shear slips, and rock breakage during the destructive process in a layered rock tunnel.
2. The presence of a weak face notably influences the damage characteristics of the surrounding rock in the tunnel. In layered rock mass scenarios, cracks no longer originate

uniformly from the tunnel's edge, but instead initiate from the joint surface. This results in a rearward shift of the shear surface, consequently expanding the range of damage zones. The joint angle significantly impacts the distribution pattern of cracks, which consistently concentrate in a direction perpendicular to the joint surface. Moreover, in the context of a layered rock tunnel, a smaller rock layer thickness corresponds to a larger area of rock damage.

3. The predominant damage mode in the surrounding rock of the tunnel is primarily characterized by shear damage. The existence of a joint surface diminishes the occurrence of shear damage. An increase in the angle of the joint surface results in an initial rise followed by a decrease in the number of cracks, indicating a U-shaped trend. Moreover, a reduction in the thickness of the rock layer correlates with an increase in the number of cracks and a decrease in the proportion of shear-related cracks.

References

[1] J. Zhu, H. Wei, X. Yang, and H. Chu, "Prediction of Blasting Vibration Velocity of Layered Rock Mass under Multihole Cut Blasting", *Shock and Vibration*, vol. 2021, pp. 1–10, 2021, doi: 10.1155/2021/5511190.

[2] P. Cheluszka, "Excavation of a Layered Rock Mass with the Use of Transverse Cutting Heads of a Roadheader in the Light of Computer Studies", *Archives of Mining Sciences*, vol. 63, no. 4, pp. 871–890, 2018, doi: 10.24425/ams.2018.124981.

[3] J. Yang, H. Chen, X. Liangxiao, Z. Xu, T. Zhou, and C. Yang, "Analysis of uniaxial compression of rock mass with parallel cracks based on experimental study and PFC2D numerical simulation", *Archives of Civil Engineering*, vol. 68, no. 1, pp. 111–128, 2022, doi: 10.24425/ace.2022.140159.

[4] W. Jing, Y. Gao, R. Jin, and L. Jing, "Deformation failure analysis and identification method of zoning type of actual tunnel surrounding rock", *Archives of Civil Engineering*, vol. 69, no. 4, pp. 549–571, 2023, doi: 10.24425/ace.2023.147676.

[5] D. Yin, S. Chen, B. Chen, and Z. Xia, "Simulation Study on Strength and Failure Characteristics of Coal-Rock Composite Sample with Coal Persistent Joint", *Archives of Mining Sciences*, vol. 64, no. 3, pp. 609–623, 2019, doi: 10.24425/ams.2019.129372.

[6] P. Wang, C. Ma, C. Liu, Q. Liu, Y. Fu, and M. Cai, "Anisotropic behavior of excavated layered rock mass subjected to compression considering the joint roughness", *Bulletin of Engineering Geology and the Environment*, vol. 82, art. no. 373, 2023, doi: 10.1007/s10064-023-03400-3.

[7] P. Wang, M. Cai, and F. Ren, "Anisotropy and directionality of tensile behaviours of a jointed rock mass subjected to numerical Brazilian tests", *Tunnelling and Underground Space Technology*, vol. 73, pp. 139–153, 2018, doi: 10.1016/j.tust.2017.12.018.

[8] Z. Chen, C. He, G. Xu, G. Ma, and D. Wu, "A Case Study on the Asymmetric Deformation Characteristics and Mechanical Behavior of Deep-Buried Tunnel in Phyllite", *Rock Mechanics and Rock Engineering*, vol. 52, no. 11, pp. 4527–4545, 2019, doi: 10.1007/s00603-019-01836-2.

[9] Z. Guo, J. Fan, F. Wang, H. Zhou, and W. Li, "Geomechanical Model Experiment Study on Deformation and Failure Mechanism of the Mountain Tunnel in Layered Jointed Rock Mass", *Advances in Civil Engineering*, vol. 2021, pp. 1–19, 2021, doi: 10.1155/2021/6645124.

[10] Z. Sun, D. Zhang, Y. Hou, N. Huangfu, M. Li, and F. Guo, "Support Countermeasures for Large Deformation in a Deep Tunnel in Layered Shale with High Geostresses", *Rock Mechanics and Rock Engineering*, vol. 56, no. 6, pp. 4463–4484, 2023, doi: 10.1007/s00603-023-03297-0.

[11] N. Moussaei, M. Sharifzadeh, K. Sahriar, and M. H. Khosravi, "A new classification of failure mechanisms at tunnels in stratified rock masses through physical and numerical modeling", *Tunnelling and Underground Space Technology*, vol. 91, art. no. 103017, 2019, doi: 10.1016/j.tust.2019.103017.

[12] X. Sun, M. Jiang, C. Miao, J. Wang, and J. Zhang, "Study on large deformation and failure mechanism of deep buried stratified slate tunnel and control strategy of high constant resistance anchor cable", *Engineering Failure Analysis*, vol. 144, art. no. 106953, 2023, doi: 10.1016/j.engfailanal.2022.106953.

[13] X. Fang, J. Yang, X. Zhang, C. Zhang, S. Wang, and Y. Xie, "Numerical modeling of open TBM tunneling in stratified rock masses using a coupled FDM-DEM method", *Computers and Geotechnics*, vol. 156, art. no. 105251, 2023, doi: 10.1016/j.compgeo.2023.105251.

[14] Y. Li, T. Qi, B. Lei, W. Qian, and Z. Li, "Deformation Patterns and Surface Settlement Trough in Stratified Jointed Rock in Tunnel Excavation", *KSCE Journal of Civil Engineering*, vol. 23, no. 7, pp. 3188–3199, 2019, doi: 10.1007/s12205-019-0477-4.

[15] Y. Tian, X. Shu, H. Tian, L. He, Y. Jin, and M. Huang, "Effect of horizontal stress on the mesoscopic deformation and failure mechanism of layered surrounding rock masses in tunnels", *Engineering Failure Analysis*, vol. 148, art. no. 107226, 2023, doi: 10.1016/j.engfailanal.2023.107226.

[16] H. Li, Y. Zhang, H. Yin, X. Wang, W. Zhao, and W. Li, "Development of Transversely Isotropic Elastoplastic Constitutive Model in FLAC3D and Its Application in Tunnel Engineering", *Geofluids*, vol. 2022, pp. 1–15, 2022, doi: 10.1155/2022/3264675.

[17] N.A. Do, et al., "Behavior of noncircular tunnels excavated in stratified rock masses – Case of underground coal mines", *Journal of Rock Mechanics and Geotechnical Engineering*, vol. 11, no. 1, pp. 99–110, 2019, doi: 10.1016/j.jrmge.2018.05.005.

[18] P.F. Yin, S.Q. Yang, F. Gao, et al., "Application of different joint models in stratified composite rock DEM simulation", *Journal of Mining and Safety Engineering*, vol. 40, no. 1, pp. 164–173+183, 2023, doi: 10.13545/j.cnki.jmse.2021.0706.

[19] S.Y. Wang, S.W. Sloan, C.A. Tang, and W.C. Zhu, "Numerical simulation of the failure mechanism of circular tunnels in transversely isotropic rock masses", *Tunnelling and Underground Space Technology*, vol. 32, pp. 231–244, 2012, doi: 10.1016/j.tust.2012.07.003.

[20] P. Deng, Q. Liu, X. Huang, Y. Pan, and J. Wu, "FDEM numerical modeling of failure mechanisms of anisotropic rock masses around deep tunnels", *Computers and Geotechnics*, vol. 142, art. no. 104535, 2022, doi: 10.1016/j.compgeo.2021.104535.

[21] Q. Lin, P. Cao, G. Wen, J. Meng, R. Cao, and Z. Zhao, "Crack coalescence in rock-like specimens with two dissimilar layers and pre-existing double parallel joints under uniaxial compression", *International Journal of Rock Mechanics and Mining Sciences*, vol. 139, art. no. 104621, 2021, doi: 10.1016/j.ijrmms.2021.104621.

[22] D. Sulsky, Z. Chen, and H.L. Schreyer, "A particle method for history-dependent materials", *Computer Methods in Applied Mechanics and Engineering,* vol. 118, no. 1–2, pp. 179–196, 1994.

[23] L. Zhou, X. Li, Y. Peng, B. Xia, and L. Fang, "Material point method with a strain-softening model to simulate roof strata movement induced by progressive longwall mining", *International Journal of Rock Mechanics and Mining Sciences*, vol. 170, art. no. 105508, 2023, doi: 10.1016/j.ijrmms.2023.105508.

[24] B.W. Xia, K. Hu, Y.Y. Lu, D. Li, and Z.Y. Zhou, "Model Test Study on Influences of Layered Rock Mass Dip Angle on Stability of Deep-Buried Tunnel", *Applied Mechanics and Materials*, vol. 90–93, pp. 2363–2371, 2011, doi: 10.4028/www.scientific.net/AMM.90-93.2363.

Received: 2024-01-23, Revised: 2024-04-30